1956 National Convention

IRE Convention Record

Part 3

Electron Devices and Receivers

SESSIONS ON

Microwave Tubes
Electron Tubes
Broadcast and Television Receivers
Color Television Receivers
Color Television
Solid-State Devices

SPONSORED BY

IRE PROFESSIONAL GROUPS ON

Broadcast and Television Receivers
Electron Devices

Presented at the IRE National Convention, New York, N. Y., March 19-22, 1956

The Institute of Radio Engineers

IRE CONVENTION RECORD

1956 NATIONAL CONVENTION

PART 3 - ELECTRON DEVICES & RECEIVERS

TABLE OF CONTENTS

Session 16: Microwave Tubes
(Sponsored by the Professional Group on Electron Devices.)

Investigation of a Traveling Wave Tube with Interchangeable External Slow-Wave Structures . . . . . Allen R. Matthews, Chih Tang Sah and Karl R. Spangenberg 3
Hollow Beams in Electrostatic Fields . . . . . Lawrence A. Harris 11
Microwave Transmitter Tuning by Rapid-Interchange, Fixed-Frequency Klystrons . . . . . R. A. La Plante 19
Design and Performance of Low Noise Guns for Traveling-Wave Tubes . . . . . R. C. Knechtli and W.R. Beam 23
Backward Wave Oscillator Tubes . . . . . Warren W. Menke 30
Backward Wave Oscillators for Low Voltage Operation . . . . . W. L. Beaver 35

Session 23: Electron Tubes
(Sponsored by the Professional Group on Electron Devices.)

Image Orthicon for Pickup at Low Light Levels . . . . . A. A. Rotow 41
Heat-Flow Considerations in the Design of High-Dissipation Receiving Tubes . . . . . O. H. Schade, Jr. 50
The Hy-Tramp, A Grid Controlled High Transconductance Electron Multiplier . . . . . Willard E. Hostetler 55
A Long-Life Cathode for High Power UHF Transmitting Tubes . . . . . M. J. Slivka, R. E. Manfredi 58
A Method of Measuring Cathode Interface Impedance . . . . . W. U. Shipley 64

Session 29: Broadcast and Television Receivers
(Sponsored by the Professional Group on Broadcast and Television Receivers.)

Stability Considerations in Transistor IF Amplifiers . . . . . D. D. Holmes and T. O. Stanley 67
Application of Transistors to Battery-Powered Portable Receivers . . . . . J. W. Englund 68
Design of Double Tuned IF Transformers for Transistor Amplifiers . . . . . M. J. Hellstrom 69
Transient Response Versus Chrominance Bandwidth of Simultaneous Color Television Receivers . . . . . Baugh and H. E. Sweeney 77
A Deflection and Convergence System for Use with the Color Picture Tubes . . . . . Richard B. Gethmann 84

Session 37: Color Television Receivers
(Sponsored by the Professional Group on Broadcast and Television Receivers)

The "Chromatron" as the Basis for Low-Cost Television Receivers . . . . . R. D'Amato, R. Dressler and A. Jacobs 89
The Optimum Relative Phosphor Efficiencies . . . . . S. K. Altes 90
A New Color Television Display—The Apple System . . . . . J. S. Bryan, R. G. Clapp, E. M. Creamer, S. W. Moulton, and M. E. Partin 94

A Beam Indexing Color Picture Tube—The Apple Tube
. . . . . G. F. Barnett, F. J. Bingley, S. L. Parsons, G. W. Pratt and M. Sadowsky 101
Current Status of Apple Receiver Circuits and Components
. . . . . R. A. Bloomsburgh, W. P. Boothroyd, G. A. Fedde, and R. C. Moore 107
Recent Improvements in the 21AXP22 Color Kinescope
. . . . . R. B. Janes, L. B. Headrick, and J. Evans 113
General Electric Post Acceleration Color Tube . . . . . C. G. Lob 114
Correct Prints of Color Tube Screens . . . . . H. Heil 118
The Unipotential Mask-Focusing Colortron . . . . . N. Fyler, C. Cain, and P. Hambleton 122
Focusing Grill Color Kinescopes . . . . . E. G. Ramberg, H. B. Law, H. S. Allwine,
. . . . . D. C. Darling, C. W. Henderson, and H. Rosenthal 128
Electrets . . . . . Erik G. Linden 135
High Frequency Germanium NPN Tetrode . . . . . D. W. Baker 143
Optimum Design of Power Output Transistors . . . . . M. A. Clark 151
Investigation of Power Gain and Transistor Parameters as Functions of Temperature and
Frequency . . . . . A. B. Glenn and I. Joffe 157
High Frequency Tetrodes . . . . . R. F. Stewart, B. Cornelison and W. A. Adcock 166
Semiconductor Capacitance Amplifier . . . . . Frederick Dill, Jr., and Louis Depian 172

INVESTIGATION OF A TRAVELING WAVE TUBE WITH INTERCHANGEABLE EXTERNAL SLOW-WAVE STRUCTURES

Allen R. Matthews, Maj., USAF; WADC, Ohio
Chih Tang Sah; Stanford University, California
Karl R. Spangenberg, Prof., Stanford University, California

Summary

This report describes an investigation of a traveling wave tube using a lumped filter circuit as a slow wave structure[1]. The critical part of the slow wave structure is physically external to the vacuum envelope with direct electrical connections to a series of metal cylinders physically inside of the vacuum envelope.

The tube design, construction, beam focusing and d-c tests are discussed. Theoretical and experimental information is presented on the slow wave structure, and on the r-f operation of the tube. Three types of operation are discussed -- backward wave oscillator (BWO), backward wave amplifier (BWA), and forward wave amplifier (FWA). Tube operation is demonstrated with uniform magnetic field and periodic electrostatic beam focusing.

Experimental voltage tunable backward wave oscillator operation is described in detail for an output in excess of one watt over a frequency range from 340 to 450 mc. An r-f output of 5 watts at an efficiency of 10 percent was obtained at a frequency of 428 mc. Voltage tuning from 80 to 457 mc was obtained experimentally with minor mode interference.

Introduction

The purpose of this investigation is to determine the feasibility of traveling wave tube operation utilizing a controlling portion of the slow wave structure external to the vacuum envelope. Lumped element filter circuits were initially selected and tested. Filter helixes were also examined.

Comparison of lumped filter-type and helix-type TWT's shows that within the VHF and UHF frequency regions there are advantages and disadvantages for each type tube. However, the tube described herein has the unique feature of permitting interchange of the slow wave structure while using the same vacuum envelope. This feature permits the selection of a structure most suited to the desired operation -- oscillator or amplifier, narrow band or wide band. In addition, the external circuit properties can be varied while the tube is in operation. Furthermore, combinations of external circuits can be readily obtained for particular types of operation, such as cascade slow wave structures for BWA operation.[2]

The internal part of the slow wave structure was selected to give optimum beam coupling. A series of coaxial cylinders was selected to provide the required interaction between the external circuit wave and electron beam. Such a configuration also provides a series of electrostatic lenses that make periodic electrostatic focusing possible. Furthermore, the spacing of the cylinders can be modified during tube construction in order to permit advantageous operational results such as mode interference reduction or increased efficiency.

Tube Design, Construction, and Beam Focusing

Figure 1 shows a photograph of the experimental tube. The vacuum envelope and its subassemblies will be described separately.

The Electron Gun

The electron gun is a Pierce type electrostatically focussed gun. The gun employed a Philips type BPIA tungten pellet impregnated with barium aluminate and had a diameter of 0.120 inch. A standard 6.3 volt heater was used. The measured gun perveance was 2.8×10^{-6}. The beam current was controlled by the anode voltage. A special gun mounting was designed to center the gun coaxial with the interaction cylinders.

The Collector

An anode of the type used in the Eimac 75T tube was modified by the addition of a molybdenum disc welded inside the cylindrical surface and used as a collector. Heat dissipation of approximately 75 watts was achieved by using an Eimac HR-3 heat dissipator external to the vacuum.

Interaction Cylinders

The interaction cylinders were made of thin wall molybdenum tubing and had solid tungsten rod leads brazed thereto. Nicoro wire (gold-nickel-copper alloy) was used for the braze. The cylinders were 0.162 inch inside diameter and 0.315 inch long. The uniform spacing between cylinders was 0.078 inch. These dimensions were selected on the basis of giving a minimum reduction in beam-circuit interaction and a convenient tuning voltage range for the circuit to be tested. The modulation coefficient reduction

factor for a solid beam not filling the cylinders is the order of 0.98. The reduction factor for finite time of electron travel across the interaction gap is numerically larger than 0.9. The mechanical periodicity of the cylinder plus gap is approximately one cm. It should be noted that the external circuit connection can give an effective electrical periodicity which is a multiple of the mechanical periodicity.

Tube Assembly

The cylinders and leads were mounted in a jig and brazed in a hydrogen furnace.

Twenty-nine cylinders with leads were then assembled onto a mandrel with the pre-beaded leads extending through previously prepared holes in the glass envelope. The cylinders were accurately spaced by means of stainless steel ground spacers. The mandrel was accurately located inside of and coaxial with the 3/4 inch ID precision glass by means of temporary precision carbon bearings. Each lead was then sealed to the glass envelope.

Other methods of mounting cylinders inside of a glass envelope have since been demonstrated to offer certain advantages, although the method used for this report appears practical once the technique is mastered.

D-C Tests with Uniform Magnetostatic Beam Focusing

An experimental electromagnet was used to focus the electron beam. Magnetic field strengths from 400 to 1100 gauss were used to obtain beam transmission the order of 90 percent over a range of beam currents from one to sixty ma.

Periodic electrostatic beam focusing was tested and gave 90 percent transmission for beam currents the order of one ma. Fig. 2 shows an oscillogram of percent beam transmission versus the focusing voltage between interaction cylinders for a beam velocity corresponding to 600 volts. The focusing voltage was actually a 60 cps voltage between cylinders and superimposed upon the d-c beam voltage. The average beam voltage is therefore the voltage of a point midway between cylinders. The voltage[3] between this point and an adjacent cylinder is designated, ϕ_a. The total voltage between cylinders is designated V_{F0} and is twice ϕ_a. Note in particular (Fig. 2) that the focusing action is symmetrical, flat topped, and has critical voltages at which the percent transmission becomes zero. The symmetry of maximum transmission is adjustable by altering the beam entrance conditions.

Fig. 3 shows a plot of critical focusing voltages versus beam voltage. The largest magnitude critical voltage is defined by

$$\phi_a = V_o \qquad (1)$$

The lowest magnitude critical voltage is defined by a more complex theory discussed in the basic report[1]. Note the close agreement between theory and experiment. Also, note that there is a fixed ratio between beam voltage and focusing voltage to achieve optimum focusing.

The Slow Wave Structure

Physical Description

The individual coils for the external part of the slow wave structure are connected in series, and with tube socket pressure contacts at each junction. The coil assembly can then be plugged onto the tube.

Fig. 4 shows the schematic circuit consisting of the external and internal parts of the slow wave structure. The individual electrical elements that comprise the circuit are noted in Fig. 4. The inductance (L_1) and distributed capacitance (C_d) of each coil are critical controlling parameters along with the capacitance (C_g) between adjacent cylinders. In addition, the capacitance (C_c) of the coil to ground must be considered. The mutual inductance (M) between adjacent coils was found to be almost negligible and was reduced by staggering or right angle mounting of the coils in the external assembly. The inductance of the leads (L_2) was not negligible and had some noticeable effect on the filter performance. Either pi or tee filters can be obtained by the use of appropriate and coils.

Electrical Filter Characteristics

The performance of the filter was experimentally determined by measuring the input impedance when the filter was terminated by an open or a short circuit. The characteristic impedance was determined from these measurements.

$$Z_o = \sqrt{Z_{oc}\, Z_{sc}} \qquad (2)$$

The phase shift per filter section was determined from a plot of frequency for short-circuit impedance versus the pole number and agreed with theory as calculated from the filter parameters.

The electrical parameters of the filter were measured separately and calculated from the filter performance data. The two methods gave similar results.

L_1	0.274 microhenry
C_1	0.1 micro-microfarad
C_2	1.35 micro-microfarad

The filter is seen to be a m-derived low pass filter with electron beam interaction gaps in the shunt filter condenser position. The filter characteristics are as follows:

f_c	457 mc
R_o (Z_o at f = o)	450 ohms
m	0.88

The insertion loss of the filter over the frequency range 250 to 450 mc was the order of 0.3 db per filter section.

Broadband impedance matching of the filter to a 50 ohm line presented some difficulties. A tapered helix was ultimately used and was satisfactory.

The Filter As a Slow-Wave Structure

Fig. 5 shows a Brillouin diagram based upon the omega-beta curve which was obtained from the phase shift per filter section versus frequency data of the filter cold test. The forward wave and backward wave modes of TWT operation are evident by the positive or negative slope respectively of the line representing circuit wave group velocity.

Fig. 6 shows a theoretical tuning curve versus frequency for the fundamental (n = o) and higher order modes of TWT operation. The curve is on semi-log paper in order to display adequately the higher order modes. It can be noted that beam voltages from 100 to 1000 volts permit single frequency BWO operation from 250 to 457 mc.

The interaction impedance (K) can be calculated and agrees with theory as will be shown later. The theory for this derivation is included in Reference 1. The interaction impedance is a function of the circuit characteristic impedance and increases from approximately 1/4 or 1/8 (depending upon the mode) of R_o at zero frequency to infinity at the filter cut-off frequency.

Backward Wave Oscillator Operation

BWO Operation

Fig. 7 shows an oscillogram of BWO power output as a function of beam voltage. The oscillator frequency is noted on Fig. 7. This oscillogram was obtained using conventional d-c circuits with a 60 cps sweep voltage superimposed on the d-c beam voltage and uniform magnetic field beam focusing. Note that the upper oscillation frequency approximately agrees with the filter cold test cut-off frequency. The non-linear variations in power output as a function of frequency are the result of variations in impedance matching between the slow wave structure and the 50 ohm output cable. At very low beam voltage there is evidence of additional higher order mode oscillations which have been examined in detail[1].

Tuning Curves

Fig. 8 is an experimental tuning curve of beam voltage versus frequency for constant magnitude of beam current. There is close agreement between the low beam current (approximately 1 ma for start oscillation) curve and the theoretical curve based upon cold tests of the filter. A small higher order mode interference is shown. This interference is the result of a higher order mode having a larger gain parameter (C) than the lower order mode[1].

Frequency Pushing

The amount of frequency pushing is also evident from Fig. 8. A detailed experimental study of this effect[1] indicates that the amount of pushing for a fixed beam current is independent of the length of the slow wave structure or the beam current relative to start oscillation current. The beam voltage as a function of beam current for constant frequency operation can be accurately determined theoretically[1] but the relation between frequency versus beam current for constant voltage is not as easily derived. An empirical relation was obtained from the experimental data.

$$\frac{f_o - f}{f_o} = \frac{106}{V_o^{5/4}} (1 - I_o^{1/3}) \text{ percent} \quad (3)$$

where f_o is the frequency at zero beam current and the other notation is standard (volts and milliamperes). In all cases, the frequency decreased with increased beam current.

Start Oscillation Current

Extensive data of start oscillation current (I_s) versus frequency and circuit length was obtained and agreed with theory. For example, I_s was found to be proportional to the inverse cube of the number of filter sections.

Gain Parameter

Fig. 9 shows the variations of the gain parameter C versus frequency. The value of C was calculated from values of $(CN)_{st}$ published by Johnson[4] and considered the effect of space charge, circuit attenuation, and velocity parameter (b). Some theoretical curves are shown for low and high space charge. Additional data verified the variation of C as the inverse function of length[1]. Values of C of the order of 0.15 were obtained.

Interaction Impedance

Fig. 10 is included to show the relation between the interaction impedance K and frequency. The experimental and theoretical curves are in close agreement. The value of K varies smoothly from 50 to 750 ohms over a frequency range from 200 to 450 mc. The experimental values of K were obtained from the relation,

$$C^3 = K \frac{I_s}{4 V_o} \quad (4)$$

Minor variations of K as a function of length were noted and are believed to be primarily due to experimental error.

Power Output

Fig. 11 shows the oscillator power output as a function of normalized beam current. A family of curves, each one for a constant circuit length, are shown. For normalized beam currents larger than 3, the power output varies approximately as the 4/3 power of normalized beam current which is an approximate theoretical variation[1]. The power output as a function of length was shown[1] to vary as the inverse 4.5 power of the number of filter sections in comparison with the theoretical 4th power[1].

Fig. 12 shows the variation of power output as a function of frequency for two values of constant beam current. The power output inherently decreases with frequency because the beam voltage is less at lower frequencies. For this reason a curve is also shown for constant beam power and indicates that power output increases with decreasing frequency. An additional test of power output versus circuit length for constant beam power indicates that there is a critical circuit length for maximum output[1]. The critical length is also a function of the beam power but to a lesser degree.

Electronic Efficiency

The electronic efficiency was examined in detail[1] and found to be in approximate agreement with the work of Grow[5]. The fundamental factors of circuit loss, velocity spread, large C, and gap field variations were included to correct the experimentally measured efficiency. The corrected efficiency was then found to vary linearly and to be approximately equal to the value of C. Measured efficiencies of the order of 10 percent were obtained.

Periodic Electrostatic Beam Focusing

As previously indicated, such focusing was first examined without any r-f on the beam. Tests of r-f operation with this type of beam focusing were conducted.

Tuning Curves. Fig. 13 is a tuning curve showing a comparison between the periodic electrostatic focusing case and the theoretical tuning curve which has already been compared to the uniform magnetic field beam focusing case. It must be carefully noted that alternate cylinders are at different voltages with respect to the cathode. These voltages are indicated as V_{01} and V_{02} and plotted in Fig. 13. In addition, another curve is shown on Fig. 13 and closely agrees with theoretical tuning curve. The difference is only due to frequency pushing. The additional curve is based upon the following relation between V_{01} and V_{02}.

$$V_0 = \sqrt{V_{01}\ V_{02}} \qquad (5)$$

A variety of tests confirmed this relation.

Power Output

Fig. 14 shows a comparison of oscillator power output for the two methods of beam focusing and includes a correlation with percentage beam transmission. The purpose of this figure is to demonstrate that the tube operates equally well with either type beam focusing. The power output is limited in the periodic electrostatic focusing case only by the amount of beam current that can be so focussed.

Amplifier

Backward Wave Amplifier

The same external filter circuit was examined as a BWA including the region of transition from BWA to BWO[1]. This slow wave structure provides narrow band amplification the order of 6 mc bandwidth between -3 db gain points at a center frequency of 427 mc. The electronic gain versus normalized beam current increased with increasing normalized beam current from zero gain to a value the order of 4 db for large signal (+20 dbm) input to the order of 24 db for small signal (-20 dbm) input. For signal inputs the order of 0 dbm, the gain was approximately defined by the relation,

$$\text{voltage gain} \sim 20 \log \frac{1}{1 - I_o/I_s} \text{ db} \qquad (6)$$

Forward Wave Amplifier

FWA operation was examined[1] for 14 filter sections at only one frequency, 450 mc, due to voltage limitations of the experimental arrangement. The performance is accurately described by the basic relation,

$$G = A + BCN \text{ db} \qquad (7)$$

The experimental evaluation of these parameters gave the following values:

$G = 4$ db ($I_o = 1$ ma.)
$A = -9.5$
$B \sim 41$
$C = 0.0685$ ($I_o = 1$ ma.)
$N = 4.8$

The gain is proportional to the one third power of beam current. Electronic gain the order of 25 db can theoretically be obtained by increased tube length and/or beam current.

This slow wave structure gives narrow band operation. The bandwidth for -3 db gain is 6 mc at a center frequency of 450 mc. Additional tests on another slow wave structure plugged onto the same tube gave wideband FWA operation from 250 to 350 mc, thus demonstrating the versatility of the tube in providing desired operational characteristics.

Conclusions

A traveling wave tube using a controlling portion of the slow wave structure external to the vacuum envelope has been demonstrated. The performance is in accordance with existing theories and provides characteristics of practical importance. Within the VHF and UHF frequency regions, this tube offers certain advantages over the conventional helix types of TWT's. For example, the optimum BWO lumped circuit tube design, giving an output in excess of one watt at an efficiency in excess of four percent over a frequency range from 340 to 450 mc, is only 3 inches long and of small diameter depending upon the coil arrangement. This tube is inherently suited for periodic electrostatic or uniform magnetic focusing systems.

The internal portion of the slow wave structure can be easily modified for a tapered periodicity or even a periodic variation of the basic periodicity. Improvements in efficiency and higher order mode elimination are therefore possible. The size of the cylinders or other internal electrodes can be modified to accommodate various configurations and sizes of electron beams and to control the coupling between the circuit wave and electron beam. A variety of mechanical arrangements are possible for simultaneously providing external electrical connection and mechanical mounting of the internal electrodes.

The external portion of the slow wave structure can be of a wide variety of types -- lumped filters, filter helixes, or tuned lines. Slow wave structures can be conveniently used in several arrangements such as in cascade[2]. In addition, multifunction tubes are possible by appropriate arrangement of the external slow wave structures. The electrical characteristics of the external portion can also be modified while the tube is in operation. For example, the use of tunable inductors would permit the cut-off frequency of the tube to be changed over an appropriate range while still permitting voltage tuning near the cut-off frequency. This procedure permits continuous operation near the filter cut-off frequency which then gives improved performance and a wider overall tuning range. Individual external sections can also be individually tuned for modifications in the gain performance or possibly increased efficiency by a tapered slow wave structure.

Additional investigations on this type of TWT are underway at Stanford University and will be reported upon in the future.

References

1. A. R. Matthews, "Investigation of a Traveling Wave Tube with Interchangeable External Slow-Wave Structures", Tr-No 102, N6 onr 251(07) NR 073 360, Stanford University (Electronics Research Laboratory), 7 February 1956.

2. M. R. Currie, J. R. Whinnery, "The Cascade Backward-Wave Amplifier: a High-Gain Voltage-Tuned Filter for Microwaves", IRE, November 1955, pp 1617-1631, Vol. 43, No. 11.

3. C. W. Barnes, "Periodic Focusing of Electron Beams", TR-No. 33, N6 onr 25132, Stanford University (Electronics Research Laboratory), 3 May 1954.

4. H. R. Johnson, "Backward Wave Oscillators", Proc. IRE, Vol. 43, June 1955, pp 684-697.

5. R. W. Grow, "Backward-Wave Oscillator Efficiency", TR-No 80, N6 onr 251(07), Stanford University (Electronics Research Laboratory), 2 November 1954.

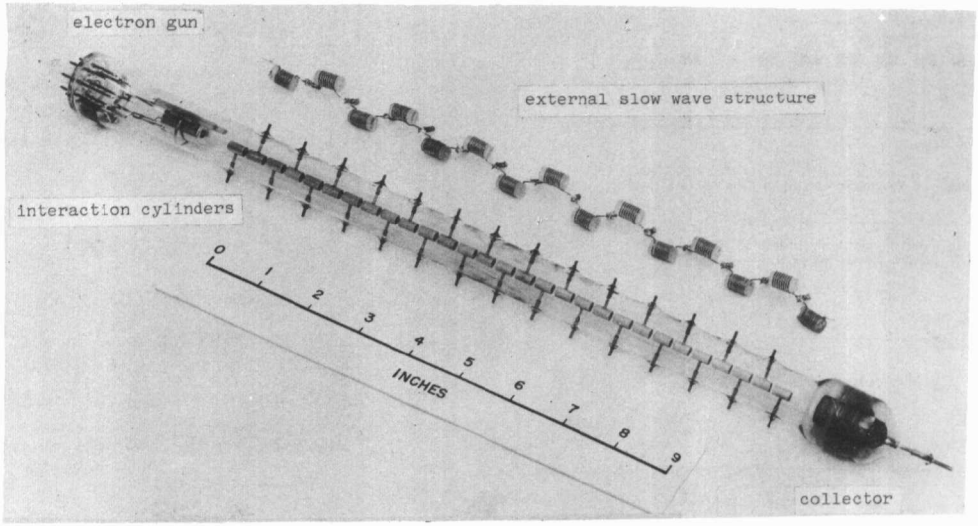

Fig. 1 (1.1[1])
Photograph of external circuit TWT No. 7A-5501-1A

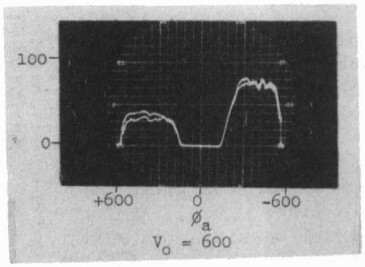

Fig. 2 (2.17[1])
Oscillogram of beam current percentage transmission with periodic electrostatic focusing (I_o = 1.0 ma)

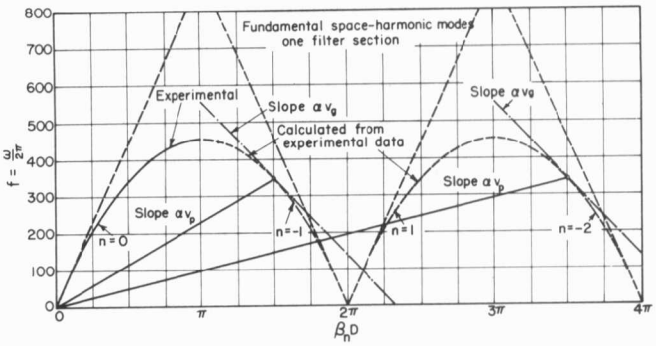

Fig. 5 (3.9[1])
Brillouin diagram for experimental slow-wave structure.

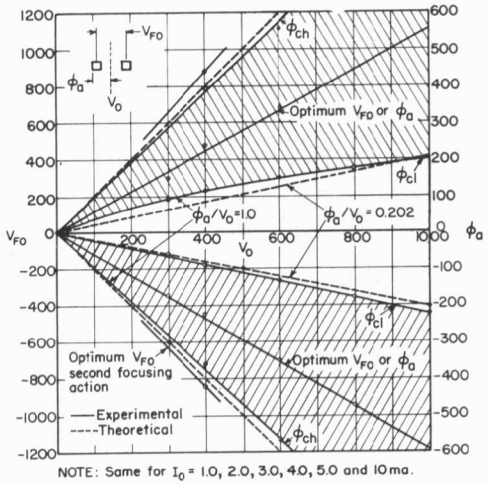

Fig. 3 (2.18[1])
Periodic electrostatic focusing voltage as a function of beam voltage

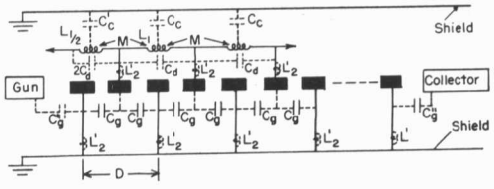

a. Lumped-Parameter Equivalent Circuit of Slow-Wave Structure.

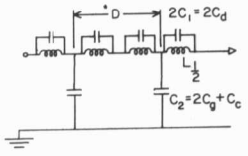

b. T m-derived Filter Sections

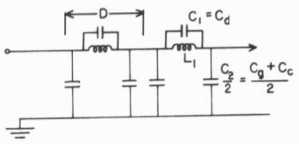

c. π m-derived Filter Sections

Fig. 4 (2.2[1])
Schematic circuit of slow-wave structure

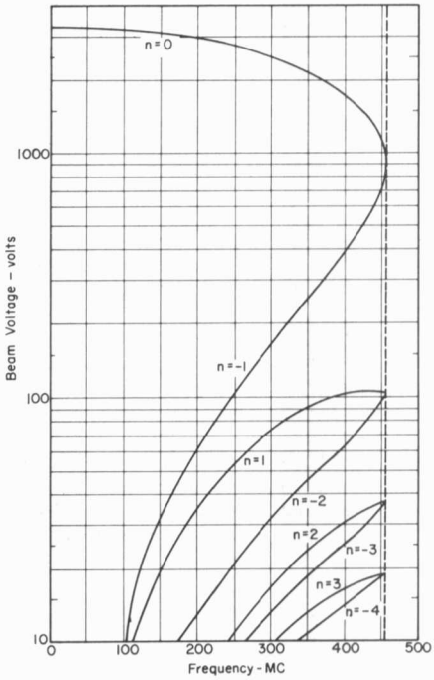

Fig. 6 (3.11[1])
Theoretical tuning curve based upon the experimental ω-β curve for the n = 0 mode

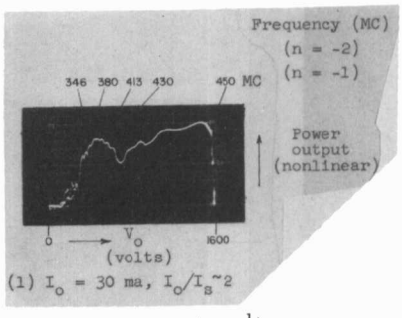

Fig. 7 (4.2[1])
Typical oscillogram of BWO operation showing power output vs beam voltage (output transformer is a tapered helix)

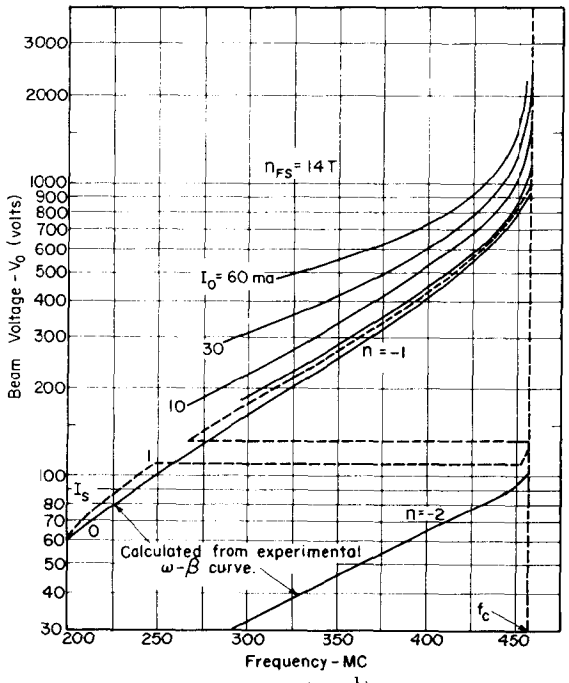

Fig. 8 (4.4[1])
BWO tuning curves for constant beam current

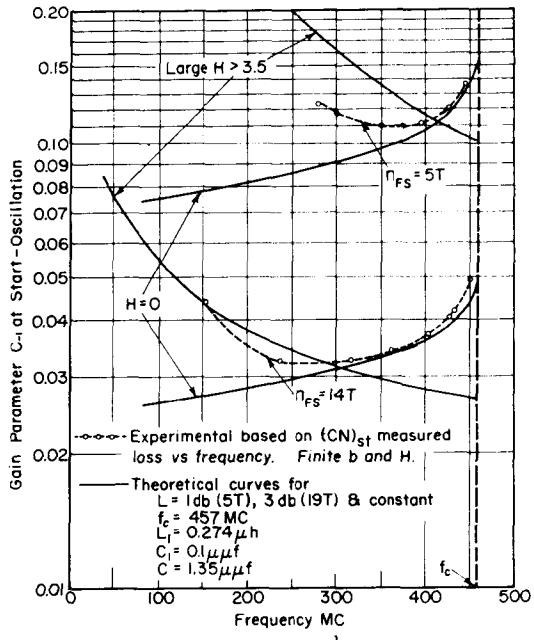

Fig. 9 (4.11[1])
Variation of the gain parameter, C_{-1}, with frequency for constant circuit length

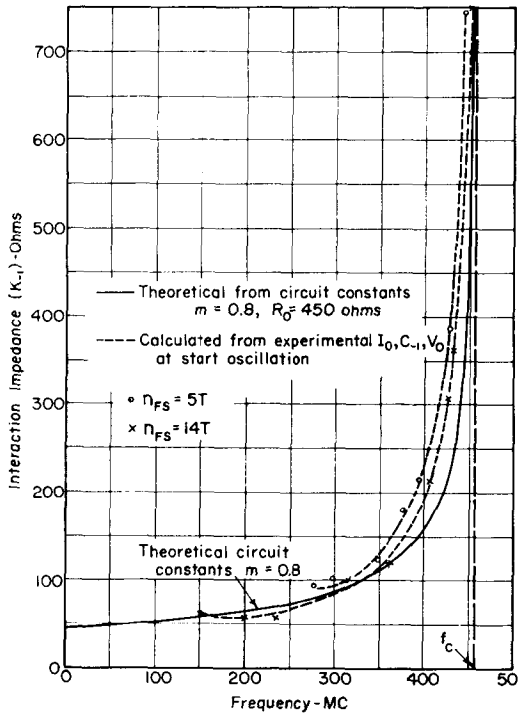

Fig. 10 (4.14a[1])
BWO interaction impedance, K_{-1}, as a function of circuit length

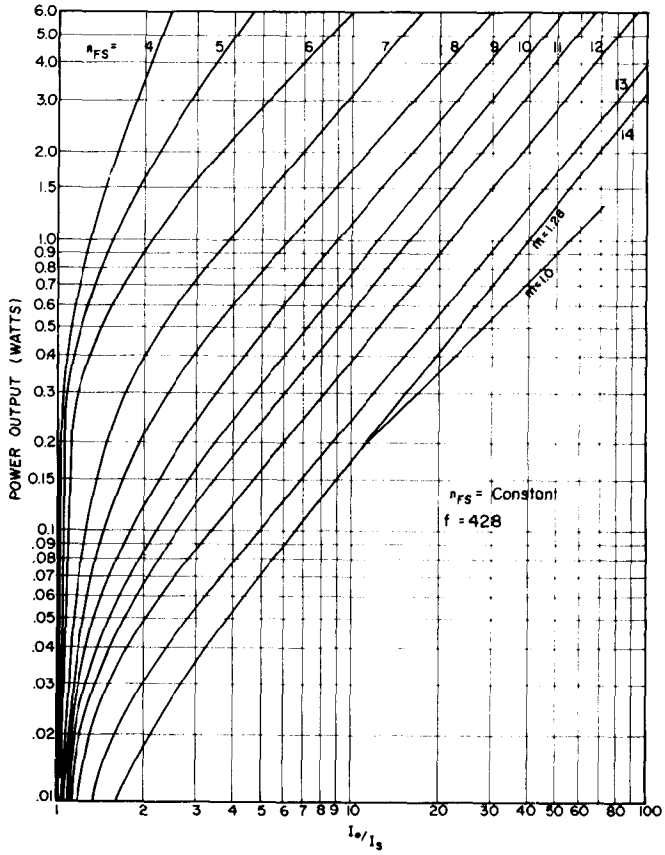

Fig. 11 (4.15[1])
BWO power output as a function of normalized beam current for constant circuit length and oscillator frequency

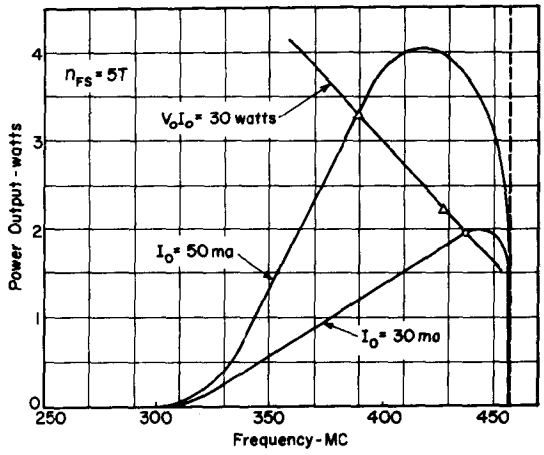

Fig. 12 (4.18[1])
BWO power output as a function of frequency for constant beam current

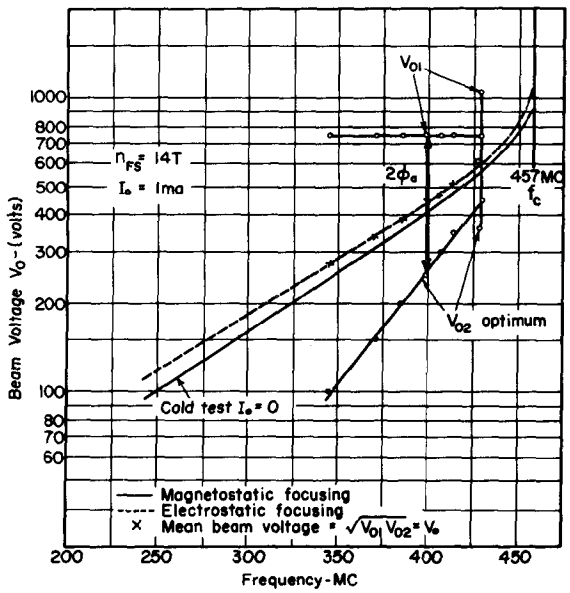

Fig. 13 (4.25[1])
BWO tuning curve with electrostatic beam focusing

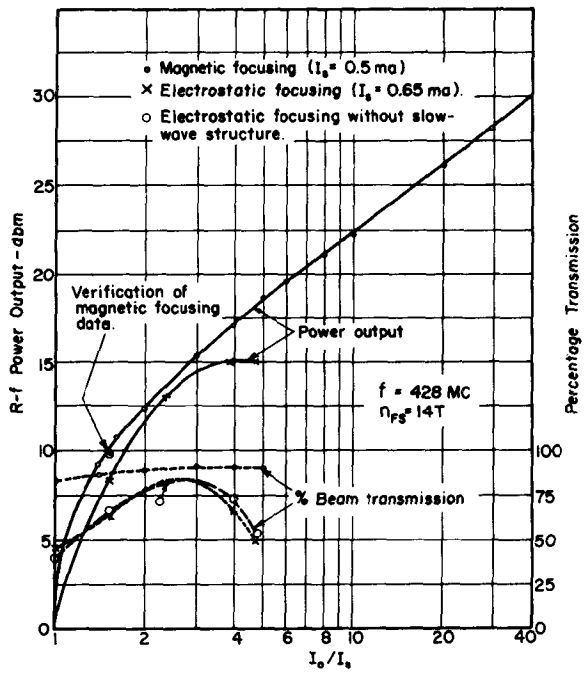

Fig. 14 (4.26[1])
BWO power output with electrostatic beam focusing

HOLLOW BEAMS IN ELECTROSTATIC FIELDS

Lawrence A. Harris
University of Minnesota*
Minneapolis 14, Minnesota

Summary

Trajectories are calculated for the inner and outer edges of tubular electron beams in radial electrostatic fields. The beams are assumed to be initially of zero thickness and to have uniform axial velocity. Special cases considered include that of a beam inside a single drift tube and a beam between coaxial drift tubes. Both diverging and converging beams are treated in strong and weak radial fields. It is shown that strong radial fields effectively reduce the space-charge spread and at the same time deflect the beam. Calculated results for a particular beam are presented as an example for each of these cases.

Introduction

The use of hollow or tubular electron beams is indicated in beam-type microwave tubes requiring large currents and high efficiencies. Methods for maintaining uniform radius and thickness of hollow beams have been previously described[1]. One system of interest requires that a magnetic shield be placed over the electron gun or over the beam. The gun produces a hollow beam which then passes through a short transition region containing a radial magnetic field and then enters the space between coaxial drift tubes where it is put to use (Fig. 1). It is in the transition region that electrons acquire an angular velocity to produce a centrifugal force in the remainder of the system between drift tubes. This force and the space-charge force are balanced by the applied electric force due to the voltages on the drift tubes.

In such a system there is usually some space in which the electrons travel without rotation between the gun and transition region. This space may be longer than mechanical considerations demand in order to keep the gun remote from the fringing fields of the transition region. It is the purpose of this paper to consider the motion of the electron stream in this space, called the electrostatic drift region in Fig. 1, where it is subject to electrostatic forces alone.

The motion of the beam in this space determines the entrance conditions to the transition region; conversely, if these are specified the required exit conditions at the electron gun anode are determined by the beam motion. It is assumed here that the entrance conditions to the transition region are known from design specifications. In the absence of magnetic fields the reversibility of electron paths may be employed to trace the trajectories back to the gun anode. In what follows it is also assumed that axial symmetry exists and that all electrons have the same axial velocity.

Before entering a discussion of the beam trajectories one important characteristic of hollow beams should be noted. This is the possibility of producing a ring crossover at which the inner and outer beam edges meet or intersect if thermal velocity spread is neglected. A crossover implies an infinite space-charge density but only in an infinitesimal region. The forces tending to prevent such an occurrence are note infinite however, and may be easily overcome by electrons with sufficient initial momenta properly directed. The crossover is similar to that possibld in a sheet beam, the hollow beam being essentially a sheet beam rolled into a tube[2]. With finite radius and axial symmetry the forces remain finite.

A limiting case of particular interest occurs when the beam edges meet but do not cross. In this case the beam forms a short ring of zero thickness in which all electrons have only axial velocities. This is the condition assumed to exist at the entrance to the transition region.

Analysis

The various radii used in the discussion are r_1 the inner electrode radius, r_a the inner beam edge radius, r_o the entrance radius described above, r_b the outer beam edge radius and r_2 the outer drift tube radius. The potentials applied to the inner and outer drift tubes are ϕ_1 and ϕ_2 respectively. The total beam current is I (negative) and the potential determining the axial beam velocity is V, $\dot{z} = (-2eV/m)^{1/2}$ where m is the electron mass and e is the electron charge (negative).

*Now with General Electric Research Laboratory
Schenectady, New York

The first case is that of a hollow beam inside one drift tube but with no inner drift tube present. The entire space enclosed by the beam is at a constant potential and there is no electric field there. The inner beam edge therefore remains at a constant radius $r_a = r_o$. The outer beam edge expands due to the space-charge forces produced by the charges of the beam itself. If Q is the total beam charge per unit length then

$$Q = I/(-2^{eV}/m)^{1/2} \tag{1}$$

The radial force is

$$eE = eQ/(2\pi\epsilon r_b) = m\ddot{r}_b \tag{2}$$

where ϵ is the permittivity of free space.

This equation may be integrated twice to yield the familiar beam spread curve reproduced here for completeness[3]. The slope of the outer edge of the beam is also represented in Fig. 2.

There is one difference between the case just considered and that of the usual spreading of a solid beam. In the solid beam the charge density in the cross section is assumed uniform and the forces on different electrons in the beam are proportional to their initial radii. It follows from this that all trajectories are similar in form except for different radial scale factors and the uniform charge density is maintained as the beam spreads. In the hollow beam this is not true and attention is restricted only to the inner and outer beam edges.

If the axial velocity is specified by the potential V, then the potential ϕ_2 on the enclosing drift tube is calculated by integrating the electric field from beam to drift tube

$$\phi_2 = V - \int_{r_o}^{r_2} \frac{Q\,dr}{2\pi\epsilon r} = V - \frac{Q}{2\pi\epsilon} \ln \frac{r_2}{r_o} \tag{3}$$

The motion of the beam between coaxial electrodes held at fixed potentials is more complex. Here both the inner and outer edges are subject to radial electric forces; the inner edge experiencing a force due to the total charge per unit length q induced on the inner electrodes by the beam and by the applied potentials. The outer edge experiences the same force in addition to that due to the beam charge Q itself. The difficulty in the analysis comes about because the charge q depends not only on the applied voltages and the beam charge Q but also on the effective radial position of the beam.

If the beam lies between radii r_a and r_b and has a uniform charge density

$$\rho = Q/\pi (r_b^2 - r_a^2) \tag{4}$$

in its cross section, then it can be shown by solving Laplace's and Poisson's equations in the appropriate regions, that

$$q = -\frac{2\pi\epsilon(\phi_2-\phi_1)+Q\left[\ln \frac{r_2}{r_b} + \frac{1}{2} - \frac{r_a^2 \ln r_b/r_a}{r_b^2 - r_a^2}\right]}{\ln \frac{r_2}{r_1}} \tag{5}$$

The limit of this expression as r_a and r_b both approach the effective radius r_e is

$$q = -(\ln r_2/r_1)^{-1}\left[2\pi\epsilon(\phi_2-\phi_1) + Q \ln r_2/r_e\right] \tag{6}$$

In this limiting case the entire beam is assumed to be concentrated in a thin shell at r_e. By equating the two expressions for q one finds the equivalent radius at which a thin beam induces the same charge on the inner electrode as a thick one does. This process yields

$$r_e/r_a = \exp(-1/2)\,(r_b/r_a)^{r_b^2/(r_b^2-r_a^2)} \tag{7}$$

If r_e/r_a is plotted versus $(r_b-r_a)/2r_a$ it is found that in the range of interest

$$r_e/r_a \approx 1 + (r_b-r_a)/2r_a \tag{8}$$

or

$$r_e = (1/2)\,(r_a+r_b) \tag{9}$$

to a very high degree of accuracy. This approximation for re is used in all that follows.

Equation 6, when equation 9 is substituted into it, becomes

$$q = -\frac{2\pi\epsilon(\phi_2-\phi_1) - Q \ln \frac{r_a + r_b}{2r_2}}{\ln \frac{r_2}{r_1}} \tag{10}$$

It is now a simple matter to write the equations of motion for the two beam edges,

$$\ddot{r}_a = e\,q/(m\,2\pi\epsilon\,r_a) \tag{11a}$$

$$\ddot{r}_b = e(q+Q)/(m\,2\pi\epsilon\,r_b) \tag{11b}$$

which become on substitution of equation 10

$$\ddot{r}_a = (a/r_a)+(b/r_a)\ \ln\left[(r_a+r_b)/2r_2\right] \qquad (12a)$$

$$\ddot{r}_b = (a/r_b)+(b/r_b)\ \ln\left[(r_a+r_b)/2r_1\right] \qquad (12b)$$

where

$$a = -e(\phi_2-\phi_1)/(m \ln r_2/r_1) \qquad (13a)$$

$$b = e\ Q/(m\ 2\pi\epsilon \ln r_2/r_1) \qquad (13b)$$

It is convenient to normalize all radii with respect to r_o, making equations 12 read

$$\ddot{R}_a = (a/r_o^2R_a)+(b/r_o^2R_a)\ \ln\left[(R_a+R_b)/2R_2\right] \qquad (14a)$$

$$\ddot{R}_b = (a/r_o^2R_b)+(b/r_o^2R_b)\ \ln\left[(R_a+R_b)/2R_1\right] \qquad (14b)$$

These equations are to be integrated subject to the following conditions: at t = o, $R_a = R_b = 1$ and $\dot{R}_a = \dot{R}_b = o$.

Since R_a and R_b appear in both equations it is necessary to solve them simultaneously or to make further approximations. The latter course allows the solution to be carried out for two cases of interest. In the first, a weak applied radial field is assumed making the constant "a" small with respect to "b". Thus the space charge and its images are principally responsible for the beam motion. In the second case strong applied fields minimize the effects of space charge. The details of these approximations are discussed in the separate analyses for each.

Weak Radial Fields

The assumption that the applied radial electric field is weak is incorporated into the equations by setting r_e = constant or $R_e = 1$ in view of the initial conditions. The two equations of motion then become

$$\ddot{R}_a = A/R_a \qquad (15a)$$

$$\ddot{R}_b = B/R_b \qquad (15b)$$

where

$$A = (a - b \ln R_2)/r_o^2 \qquad (16a)$$

$$B = (a - b \ln R_1)/r_o^2 \qquad (16b)$$

For this assumption to be even approximately true the inner beam edge must decrease in radius while the outer edge increases in radius. Consequently the solution for R_a must apply where $R_a \leq 1$, and that for $R_b \geq 1$. Obviously A must be negative and B positive. Since A and B differ only in the logarithm this term must predominate in each. Thus the quantity "a", hence $(\phi_2-\phi_1)$ must be small. More precisely the following inequality must hold.

$$b \ln R_1 < a < b \ln R_2$$

or

$$-Q(\ln R_1)/(2\pi\epsilon) < (\phi_1-\phi_2) < -Q(\ln R_2)/2\pi\epsilon) \qquad (17)$$

Both equations 15 are integrated once to yield

$$-dR_a/(2\ A \ln R_a)^{1/2} = dt \qquad (18a)$$

$$dR_b/(2\ B \ln R_b)^{1/2} = dt \qquad (18b)$$

with the appropriate initial conditions.

Integration of equation 18a is obtained by letting

$$R_a = \exp(-x^2) \qquad (19)$$

This yields

$$1/2(-2A)^{1/2}\ t = \int_o^x \exp(-p^2)dp \qquad (20)$$

where p is merely a variable of integration corresponding to x.

Since the right hand integral is a tabulated one (the error function[4]) time may be plotted as a function of x or of R_a. For constant axial velocity time is proportional to axial distance z and the curve thus represents a profile of the inner edge of the beam. Thus

$$(1/2)(-2A)^{1/2}(-2eV/m)^{-1/2}\ z = \int_o^x \exp(-p^2)dp \qquad (21)$$

For design purposes the slope of the beam edge is also desirable. This is given by

$$dra/dz = dR_a/d_Z = -\ r_o(-2A)^{1/2}\ (-2eV/m)^{-1/2}\ x \qquad (22)$$

where

$$Z = z/r_o \qquad (23)$$

Integration of equation 18b is carried out similarly except that the change of variable

$$R_b = \exp(y^2) \qquad (24)$$

is made, yielding

$$(1/2)(2B)^{1/2}\ (-2eV/m)^{-1/2}\ z = \int_0^y \exp(p^2)dp \qquad (25)$$

and the integral on the right is also tabulated[5]. The slope of the beam edge is given by

$$dr_b/d_z = dR_b/d_Z = r_o(2B)^{1/2}(-2eV/m)^{-1/2}y \qquad (26)$$

The two beam profiles represented by equations 21 and 25 are shown in Fig. 3. The horizontal scales on these profiles differ because of the differing coefficients of z. Once the constants for a given beam system are known these scales may be properly adjusted. Further normalization is not apparent.

Strong Radial Fields

If the applied radial field is strong then the space-charge forces are weak by comparison. In this case the beam remains relatively thin so that in equation 14a, R_b may be replaced by R_a, and conversely in equation 14b. The equations of motion are then written

$$\ddot{R}_a = a/(r_o^2 R_a) + \left[b/(r_o^2 R_a) \right] \ln R_a/R_2 \qquad (27a)$$

$$\ddot{R}_b = a/(r_o^2 R_b) + \left[b/(r_o^2 R_b) \right] \ln R_n/R_1 \qquad (27b)$$

These equations are integrated once in the usual way after multiplying by $2\dot{R}$. With the stated initial conditions the following equations are found:

$$\dot{R}_a^2 = \frac{2a}{r_o^2} \ln R_a + \frac{b}{r_o^2} (\ln R_a)(\ln \frac{R_a}{R_2^2}) \qquad (28a)$$

$$\dot{R}_b^2 = \frac{2a}{r_o^2} \ln R_b + \frac{b}{r_o^2} (\ln R_b)(\ln \frac{R_b}{R_1^2}) \qquad (28b)$$

At this point a change in variable is convenient. There are two cases to consider, each requiring a different variable change. Since it has been assumed the beam remains thin, both R_a and R_b must increase or decrease together.

If R_a and R_b both increase they are always ≥ 1 and the variable change indicated is

$$R = \exp(x^2) \qquad (29)$$

The integral expressions resulting from this substitution are

$$\frac{z}{r_o} = \frac{1}{61.5}\sqrt{\frac{\ln r_2/r_1}{G}} \int_0^{x_a} \frac{e^{p^2}\,dp}{\sqrt{p^2 + K_a^2}} \qquad (30a)$$

$$\frac{z}{r_o} = \frac{1}{61.5}\sqrt{\frac{\ln r_2/r_1}{G}} \int_0^{x_b} \frac{e^{p^2}\,dp}{\sqrt{p^2 + K_b^2}} \qquad (30b)$$

where

$$K_a^2 = 2(a/b - \ln R_2) \qquad (31a)$$

$$K_b = 2(a/b - \ln R_1) \qquad (31b)$$

and the perveance

$$G = - I/V^{3/2} \qquad (32)$$

It will be noted that K_b^2 is positive so that a real solution for z is obtained without difficulty from equation 30b. If K_a^2 becomes negative, however, a real solution to equation 30a will not exist. It is necessary to adjust the parameters therefore, to keep K_a^2 positive. This condition expressed in other terms, is

$$\phi_2 - \phi_1 > -(Q \ln R_2)/2\pi\epsilon \qquad (33)$$

What this condition means is that the applied potential difference must be greater than what would be produced by the beam charge alone. In this case both edges of the beam experience an outward force.

If R_a and R_b both decrease they are always ≤ 1 and the convenient substitution in equation 28 is

$$R = \exp(-y^2) \qquad (34)$$

which leads to the solutions

$$\frac{z}{r_o} = \frac{1}{61.5}\sqrt{\frac{\ln r_2/r_1}{G}} \int_0^{ya} \frac{e^{-p^2}\,dp}{\sqrt{p^2 + K_a^2}} \qquad (35a)$$

$$\frac{z}{r_o} = \frac{1}{61.5}\sqrt{\frac{\ln r_2/r_1}{G}} \int_0^{y_b} \frac{e^{-p^2}\,dp}{\sqrt{p^2 + K_b^2}} \qquad (35b)$$

where

$$K_a^2 = 2 (\ln R_2 - a/b) \qquad (36a)$$

$$K_b^2 = 2 (\ln R_1 - a/b) \qquad (36b)$$

Note the change of sign in these equations from equation 31.

Paralleling the previous case, both of these solutions are real only if K_b^2 is positive or if

$$\phi_1 - \phi_2 > (Q \ln R_1)/(2\pi\epsilon) \qquad (37)$$

Equations 30 and 35 have been solved and plotted in convenient form on an electronic analog computer. These solutions along with curves of the slopes of the beam edges are shown in Figs. 4, 5, 6 and 7.

Fig. 4 has certain interesting features. All of the curves are beam profiles normalized with respect to the same quantity r_o. Thus one member of the family of curves represents the outer beam edge and another the inner edge since 30a and 30b differ in form only in the constants K_a^2 and K_b^2. Reference to the definitions of these constants (equation 31) shows that

$$K_b^2 - K_a^2 = 2 \ln r_2/r_1 \qquad (38)$$

which depends only on the drift tube radii. This difference then is specified by the geometry while freedom is retained to adjust either constant by choice of the applied potentials. From the curves it is clear that the larger these constants are, the closer their corresponding curves, if the difference (38) is maintained constant. Making K^2 large means applying a large radial field. The space-charge forces are made less significant and beam spread is reduced.

Examples

The results of the theory are illustrated in this section by the profiles of a single hollow beam operating under a variety of conditions. The drift tube radii r_1 and r_2 are chosen as 0.4 cm. and 0.6 cm. respectively and r_o is taken as 0.5 cm. The beam current is 50 ma. and the beam voltage V, corresponding to the axial velocity is 300 volts, resulting in a perveance G, of 9.6×10^{-6}.

In the first case, the inner drift tube is removed and the motion of the outer beam edge is determined. This beam profile is shown by curves 1 in Fig. 9. The curves are arbitrarily extended beyond the point where the beam strikes the drift tube. In this case the proper drift tube potential ϕ_2 is 316 volts.

In the second case both drift tubes are present and are held at the same potential. The resulting beam profiles, taking account of the differing scale factors for the two beam edges, are indicated as curves 2 in Fig. 9. As was assumed in the analysis, the mean beam radius remains approximately constant. Clearly the principal effect of the inner drift tube is to deflect the beam radially inward. No significant change in the thickness of the beam is produced.

In the remaining two cases potentials are applied to the drift tubes to cause both beam edges to diverge, the case of strong radial fields. With the chosen drift tube dimensions $K_b^2 - K_a^2 = 0.810$.

If K_b^2 is taken as 1, then $K_a^2 = 0.190$ and the resulting values of ϕ_1 and ϕ_2 are 287 volts and 311 volts respectively. The beam profiles are curves 3 of Fig. 9. Again, the most significant change is an outward deflection of the beam .

If K_b^2 is taken as 10, then $K_a^2 = 9.190$ and the potentials ϕ_1 and ϕ_2 become 70 volts and 488 volts respectively. The profiles are curves 4 of Fig. 8. Now in addition to a drastic change in beam deflection, there is a significant reduction in the thickness of the beam. This is particularly true if this thickness is measured normal to the electron flow, as an electron gun would see it, rather than radially.

While this radial deflection necessarily accompanies the reduction in beam spread, it is not without some advantages. It allows the electron gun to be placed well out from the axis avoiding construction problems due to lack of space near the axis. All the gun dimensions except its distance from the axis, after accounting for the lens action of the anode slit, are considerably reduced from what they would be in the undeflected case. This is due to the reduction in beam thickness and also to a reduction in the gun perveance, as distinguished from the beam perveance. The gun operates with an anode potential higher than V to provide electrons with sufficient energy to reach r_o. In high-power tubes, where very high beam densities are required, this reduction of gun perveance may be quite useful.

Conclusions

The theory and results presented here serve to formalize part of the process of hollow-beam system design. While only axially symmetric beams in electrostatic fields have been considered, the variety of special cases serves to emphasize the flexibility of hollow-beam systems in contrast to the usual solid-beam design.

This information should be particularly useful in the design of injection systems for magnetically focused hollow beams. Indeed it was for this purpose that the study was made. The case of strong applied radial fields offers particular advantages in placement of the electron gun and reduction of its perveance. Moreover, it provides some measure of flexibility in electrically controlling r_o, the injection radius.

In passing one might note the possible application of hollow beans with two crossover rings to high-power two-cavity klystrons. One difficulty with this notion is that the two edges of the beam must then have different axial velocities if all electrons are emitted from a common cathode. This would bring about a reduction in the effective bunching due to velocity modulation.

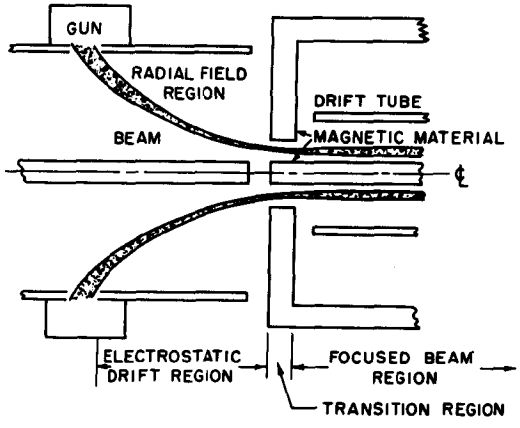

Fig. 1
Hollow beam injection system

Acknowledgement

This research was supported by the United States Air Force through the Office of Scientific Research of the Air Research and Development Command.

The author is grateful to P. N. Hess for his assistance in obtaining the results on the electronic analog computer.

References

[1] L. A. Harris, "Axially Symmetric Electron Beam and Magnetic Field Systems", Proceedings of I.R.E. v 40, 1952, pp 700-708

[2] J. R. Pierce, "Theory and Design of Electron Beams", (Second Edition, D. van Nostrand Co., New York 1954) p 151

[3] K. R. Spangenberg, "Vacuum Tubes" (McGraw-Hill Co., New York 1948) pp 440-446

[4] Jahnke and Emde, "Tables of Functions" (Dover Publications, New York, 1945) p 23.

[5] Jahnke and Emde, Loc. cit. p 32

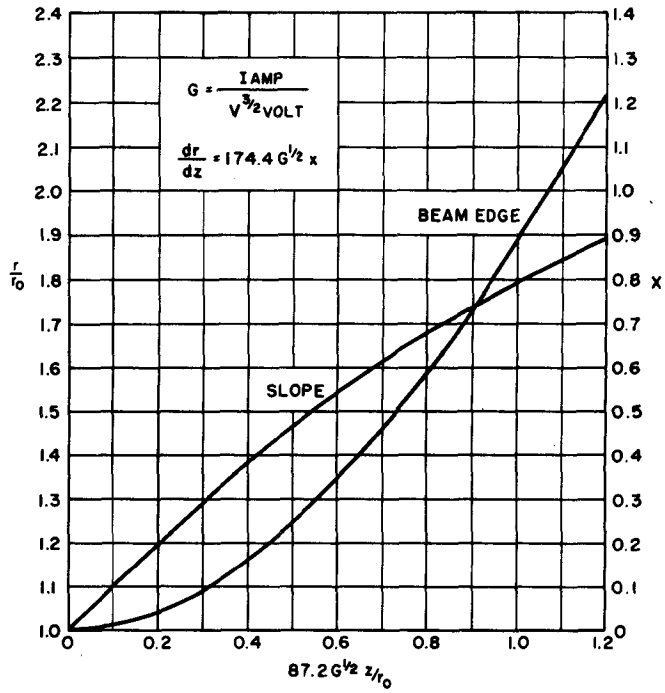

Fig. 2
Beam spread curve, inner electrode absent